

Organic Matter Amendment and Plant Colonization Drive Mineral Weathering, Organic Carbon Sequestration, and Water-Stable Aggregation in Magnetite Fe Ore Tailings

Songlin Wu,^{†,ID} Yunjia Liu,[†] Jeremy J. Bougoure,[‡] Gordon Southam,[§] Ting-Shan Chan,^{||} Ying-Rui Lu,^{||} Shu-Chih Haw,^{||} Tuan A. H. Nguyen,^{†,ID} Fang You,[†] and Longbin Huang^{*,†,ID}

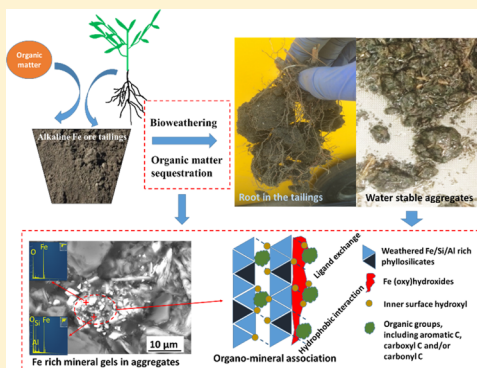
[†]Centre for Mined Land Rehabilitation, Sustainable Minerals Institute, The University of Queensland, Brisbane, Queensland 4072, Australia

[‡]Centre for Microscopy, Characterisation and Analysis, University of Western Australia, 35 Stirling Hwy, Crawley 6009, Australia

^{||}National Synchrotron Radiation Research Centre, Hsinchu Science Park, Hsinchu 300, Taiwan

Supporting Information

ABSTRACT: The formation of water-stable aggregates in finely textured and polymineral magnetite Fe ore tailings is one of the critical processes in eco-engineering tailings into soil-like substrates as a new way to rehabilitate the tailings. Organic matter (OM) amendment and plant colonization are considered to be effective in enhancing water-stable aggregation, but the underlying mechanisms have not yet been elucidated. The present study aimed to characterize detailed changes in physicochemistry, Fe-bearing mineralogy, and organo-mineral interactions in magnetite Fe ore tailings subject to the combined treatments of OM amendment and plant colonization, by employing various microspectroscopic methods, including synchrotron-based X-ray absorption fine structure spectroscopy and nanoscale secondary ion mass spectroscopy. The results indicated that OM amendment and plant colonization neutralized the tailings' alkaline pH and facilitated water-stable aggregate formation. The resultant aggregates were consequences of ligand-promoted bioweathering of primary Fe-bearing minerals (mainly biotite-like minerals) and the formation of secondary Fe-rich mineral gels. Especially, the sequestration of OM (rich in carboxyl, aromatic, and/or carbonyl C) by Fe-rich minerals via ligand-exchange and/or hydrophobic interactions contributed to the aggregation. These findings have uncovered the processes and mechanisms of water-stable aggregate formation driven by OM amendment and plant colonization in alkaline Fe ore tailings, thus providing important basis for eco-engineered pedogenesis in the tailings.



1. INTRODUCTION

The extraction and processing of iron (Fe) ores as important economic commodities have generated huge quantities of polymineral tailings with biologically hostile physicochemical properties that prohibit natural colonization of soil microbe and plants.¹ Conventional methods, by simply using large volumes of soil excavated from offsites to cover thousands of hectares of tailing landscapes, are not only expensive but also constrained by the shortage of natural soil resources and additional costs for rehabilitating the local environment destroyed by the soil excavation. Eco-engineering tailings into “soil” (or “technosol”) is a technology to rehabilitate tailing landscapes of relatively low pollution risks,^{2,3} which purposely accelerates site-specific pedological processes for the rehabilitation of biogeochemical functions to support long-term growth and development of plants and microbial communities.² Magnetite Fe ore tailings are alkaline ($\text{pH} > 9.0$) and rich in Fe-bearing primary minerals such as biotite but lack soil-like physical structure [mainly water-stable aggregate (WSA)] and organic matter (OM).¹ One of the critical barriers

to the formation of soil-like structure to possess functional biogeochemical processes is the development of WSAs in the tailings.⁴

WSAs are important building blocks of soil systems that provide physical spaces for regulating hydraulic processes (e.g., water infiltration and retention) and biological processes (e.g., microbial and plant development).⁵ In natural soil, the aggregate formation usually relies on the mineralogy resulting from millions of years of weathering and organic properties from relatively recent biological activities.^{6,7} Clay minerals including Fe-/Al-/Si-rich secondary phyllosilicates contribute critically to maintaining aggregate microstructure stability and function.⁸ Besides, secondary Fe (oxy)hydroxides contribute to soil aggregation via their association with Al-/Si-rich minerals⁹ or organic groups¹⁰ (i.e., organo-mineral association forma-

Received: July 26, 2019

Revised: November 5, 2019

Accepted: November 7, 2019

Published: November 7, 2019

tion). OM amendment is a key process to increase the labile OM level and improve the physicochemical conditions in the substrate.¹¹ For example, our previous studies found that sugarcane mulch amendment improved the physicochemical properties of Pb–Zn tailings and increased the WSA formation.¹² Organic molecules derived from decomposition of added OM could act as organic cements to interact with secondary minerals for tailing aggregation.^{13,14} The secondary minerals and OMs are largely lacking in primary mineral dominant tailings, such as Fe ore tailings.⁴ Thus, the key to overcome the fundamental barrier in eco-engineering tailings into soils is to accelerate the mineral weathering of primary minerals for rapid formation of secondary minerals (e.g., secondary Al-/Fe-/Si-bearing minerals) and OM sequestration (organo-mineral association) as the precursors to WSAs in the tailings.

In the tailing context, tolerant native and exotic plant species that could survive in the chemically improved tailings may be used as an effective biological mean to accelerate the processes from tailings to soils. Plant root activities play an important role in modifying soil physicochemical properties and soil structure formation.¹⁵ The roots can directly entangle and bind mineral particles together and excrete low-molecular-weight organic acids (LMWOAs) which accelerate the weathering of primary minerals and organo-mineral association,^{15,16} leading to the formation and development of stable aggregates. Besides, plant roots may cause reorientation of the mineral materials via physical force (or wetting–drying cycles) and thus promote aggregation in clay microstructures.¹⁷ In addition, plant roots also stimulate microbial weathering of primary minerals in the rhizosphere.¹⁸ In our recent field investigation, we found that *Maireana* spp. (native pioneer plant species) was the dominant species that survived in the Fe ore tailings and may have a great potential in Fe-bearing mineral weathering.¹ Another native leguminous species, *Acacia* spp., was also found to have survived well at the mine site.¹⁹ In our preliminary experiments, we found that a grass *Sorghum* spp. Hybrid cv. Silk was tolerant of elevated levels of salinity²⁰ and developed extensive fibrous roots throughout the profile of magnetite Fe ore tailings. Grass fibrous root systems generate extensive surface interactions with the tailing particles, which is beneficial to the process of eco-engineering tailings into soil, such as in slightly acidic/circumneutral Cu–Pb–Zn tailings.^{12,21} However, less information has been available on their role in the WSA formation in alkaline Fe ore tailings. Especially, there is a lack of knowledge on the plant-driven mineralogical change and organo-mineral interactions underpinning WSA development in the tailings.

The present study aims to characterize the effects of OM amendment and plant colonization with native plants of *Acacia ramulosa* and *Maireana brevifolia* and exotic plant *Sorghum* spp. Hybrid cv. Silk on physicochemical changes, aggregate structure formation, and the underlying mechanisms in alkaline magnetite Fe ore tailings. It is hypothesized that (1) OM amendment and plant colonization could accelerate mineral weathering to generate Fe-rich secondary minerals as prerequisites to water-stable aggregation and (2) the aggregate formation could result from the mineral–OM interactions between the secondary Fe-rich minerals and functional organic groups (such as carboxyl and aromatic groups). These expected Fe-bearing mineral weathering and their interactions with organic ligands were examined by using various microspectroscopic methodologies including synchrotron-

based Fe K edge X-ray absorption fine structure spectroscopy (XAFS),^{22,23} C 1s near-edge XAFS (NEXAFS),²⁴ back-scattered electron-scanning electron microscope-energy-dispersive X-ray spectrometry (BSE-SEM-EDS), and attenuated total reflectance–Fourier transform infrared (ATR–FTIR) spectroscopy analysis, as well as nanoscale secondary ion mass spectroscopy (NanoSIMS).²⁵

2. MATERIALS AND METHODS

2.1. Materials. **2.1.1. Magnetite Fe Ore Tailings.** The alkaline magnetite Fe ore tailings were collected from a dry stacking tailing storage facility at a magnetite Fe ore mine (Karara Mining Ltd) located in Western Australia. The tailings were strongly alkaline with pH around 9.5, low in organic carbon (0.15% w/w), and rich in primary minerals (biotite-like) and quartz, without aggregate structure.¹

2.1.2. OM and Plant Species. The OM used in the present study was sugarcane mulch (Oreco Group, Queensland, Australia), containing about 38.9% C and 0.5% N, with a C/N ratio of 78.4. Pioneer plant species included *A. ramulosa* and *M. brevifolia* (Nindethana Ltd., Australia) and an exotic crop species *Sorghum* spp. Hybrid cv. Silk (Pukalus's farm from Injune origin, Queensland, Australia). Seeds were germinated in Petri dishes with distilled water, from which sprouted seeds were transplanted into river sands irrigated with nutrient solution (containing N-20.8%, P-3.3%, and K-17.4%) for preculturing seedlings. *Sorghum* spp. Hybrid cv. Silk and *M. brevifolia* seedlings were cultivated in river sands for 2 months before transplantation to the tailing treatments, while *A. ramulosa* were cultivated for 3 months in river sands to facilitate root development before transplantation into the tailings because of slow root development of this woody species. The dry weights of the representative seedlings of these species were recorded at transplantation.

2.2. Experimental Design. The tailings were amended with 3% (w/w) OM (i.e., sugarcane mulch) and inoculated with soil microbial inoculum (mainly consisted of *Actinobacteria* (62.3%), *Chloroflexi* (11.46%), and *Proteobacteria* (8.45%) at phylum level as shown in Figure S1) in soil suspension (1:12 w/v soil/water ratio, and shaken for 24 h), which was a base treatment to lower the strongly alkaline pH for the viable growth of pioneer plants.²⁶ The tailing treatments were incubated at around 25 °C with 55% water holding capacity for 2 months, until pore water pH decreased from 9.5 to around 7.5. After this, plant seedlings cultivated in the river sand were transplanted to the tailing treatments,¹² which were cultivated for additional 2 months (Figure S2). Tailing treatment without OM amendment was not included for plant colonization treatment, as the strongly alkaline pH (about 9.5) in the tailings prohibited the survival of even tolerant plant species. Thus, there were five treatments in total: (1) tailings without any OM amendment or plant colonization ("T"); (2) tailings amended with 3% w/w OM ("T + OM"); (3) tailings amended with 3% w/w OM and cultivation of *A. ramulosa* ("T + OM + A"); (4) tailings amended with 3% w/w OM and cultivation of *Sorghum* spp. Hybrid cv. Silk ("T + OM + S"); and (5) tailings amended with 3% w/w OM and cultivation of *M. brevifolia* ("T + OM + M"). Each treatment had four replicates, totaling 20 pots. The plants colonized the tailings for 2 months, with water supply equivalent to 55% water holding capacity.

At the end of the treatment period, plant roots and shoots were separately sampled and washed carefully with distilled

water and then oven-dried at 70 °C for 48 h. The dry biomass of the plants was weighed and plant nutrient concentration was detected by ICP-OES (720ES, Varian Inc., Palo Alto, California, USA) after digestion by concentrated HNO₃.²⁷ Aliquots of the fresh tailings were stored in a dry-shipper precooled by liquid nitrogen and transported to Beamline O1C1 in the National Synchrotron Radiation Research Centre (NSRRC), Taiwan, for cryo-Fe K edge XAFS analysis. Part of the cryo-frozen fresh tailings was also used for cryo-SEM analysis at the Centre for Microscopy and Microanalysis, the University of Queensland. About 10 g of the fresh tailing samples were freeze-dried at -55 °C for 48 h for BSE-SEM-EDS, X-ray diffraction (XRD), and ATR-FTIR analysis. The remainders of tailing samples were air-dried for physicochemical analysis and wet sieving (water-stable aggregate assessment). After the wet sieving, the WSAs of different size class were collected, air-dried, and weighed, prior to further examination by means of NanoSIMS, BSE-SEM-EDS, Fe K edge XAFS, C 1s NEXAFS, and ATR-FTIR analysis.

2.3. Physicochemical Analysis. The pH and electrical conductivity (EC) in 1:5 water extracts were measured by using a pH electrode (TPS 900) and an EC electrode (TPS 2100). Total nitrogen (TN) contents were determined by a LECO CNS-2000 Analyzer (LECO Corporation, MI, USA). For total organic carbon (TOC), inorganic carbon in the tailings were removed by HCl pretreatment and the TOC contents were determined by a LECO CNS-2000 Analyzer. Brunauer–Emmett–Teller (BET)-specific surface area (SSA) of the tailing particles of different treatments were determined by nitrogen sorption by using a Micromeritics Tristar 3020 (Micromeritics Instrument Corporation, Norcross, GA, USA). WSAs were separated and collected by the wet-sieving method modified from Kemper and Rosenau (1986).²⁸ Briefly, three aggregate size fractions including (1) 2000–250 µm (fraction containing macroaggregates); (2) 250–53 µm (fraction containing microaggregates); and (3) <53 µm (silt and clay fraction) were separated. For each sample, 50 g of air-dried tailings were placed on the series of sieves and submerged into deionized water for 1 h to equilibrate. Then, the fractions of different sizes were separated by manually moving the sieves up and down at an amplitude of 3 cm (100 up–down cycles) for 2 min. The tailing aggregates on each sieve were collected and air-dried. The proportion of WSA of different sizes was expressed as the ratio of the dry weight of WSA to total dry weight (i.e., 50 g). The mean weight diameter (MWD) of WSAs was calculated as follows

$$\text{MWD} = \sum_{k=1}^{n+1} \frac{r_k + r_{k-1}}{2} \times m_k$$

where $k = 1, 2$, and 3 represent different fractions, $r_0 = 2000$ µm, $r_1 = 250$ µm, $r_2 = 53$ µm, and $r_3 = 0$ µm; m_k is the proportion of aggregate fractions on the k th sieve; and n is the number of sieves.

2.4. Microspectroscopic Analysis. **2.4.1. BSE-SEM-EDS Analysis.** The freeze-dried tailing samples were coated with carbon for SEM analysis by using a Hitachi SU3500 scanning electron microscope, with an accelerating voltage of 5–15 kV. Back-scattered electron (BSE) imaging was conducted under an accelerating voltage of 20 kV with a spot size of 50 nm, equipped with electron-dispersive X-ray spectroscopy (EDXS) to detect elemental intensity in the area of interests. cryo-SEM-EDS was used to further confirm the tailing mineral

morphology without freeze-drying. The fresh tailing samples were immediately fixed by plunging them into a liquid N₂ slush using the Oxford LN₂ slush-freezing apparatus to vitrify the samples, which were then placed onto the specimen stage (precooled by liquid nitrogen) of the field emission SEM JSM 7100F for SEM-EDS analysis. In addition, the microstructure of aggregates was examined using the air-dried WSAs embedded by epoxy resin and oven-cured at 60 °C, which were then polished and coated by carbon for BSE-SEM-EDS analysis by using Hitachi SU3500 SEM. Air-drying of water aggregates was widely used for characterizing aggregate microstructure,^{29,30} as it mimics the natural drying process and is considered to maintain the microstructure of aggregates for BSE-SEM-EDS analysis.

2.4.2. XRD Analysis. The freeze-dried tailing samples were ground into a fine powder (below 7 µm) for XRD analysis using a Bruker D8 DISCOVER diffractometer, with the Bragg–Brentano θ – 2θ reflecting geometry equipped with a Johansson-type focusing Ge primary monochromator and a linear silicon strip detector LynxEye (open to 2.896°). XRD spectrum data were collected between 4 and 70° with a step of 0.02°, and the XRD traces were processed using the Diffrac^{plus} Evaluation Package V3.1 (Bruker AXS, Germany) and the PDF-2 mineral database (2018 release).

2.4.3. Fe K Edge XAFS Analysis. Fe K edge (7112 eV) XAFS spectra of bulk fresh tailing samples of different treatments were analyzed under a flow of liquid nitrogen to minimize Fe redox changes during the spectra collection at Beamline 01C1 at the National Synchrotron Radiation Research Centre (NSRRC) in Taiwan. Besides, the air-dried WSAs were also collected and ground into a fine powder for Fe K edge XAFS analysis under room temperature at the same beamline. The detailed methods of Fe K edge XAFS analysis are provided in the Supporting Information.

2.4.4. C 1s NEXAFS Analysis. The air-dried water-stable microaggregate samples were ground into a fine powder and subject to C 1s NEXAFS analysis for characterizing organic C forms. Organic C standards including graphite (solely aromatic C), L-glucose (solely O-alkyl C), Na formate (solely carboxyl C), L-glutamic acid (alkyl C, carboxyl C), and *N,N'*-methylenebis (acrylamide) (rich in carbonyl C) were also used for verifying the organic C forms. All those standards were purchased from Sigma-Aldrich (Castle Hill, NSW, Australia). The spectra were acquired from 272 to 317 eV in the total electron yield mode (an energy resolution of 0.01 eV and an X-ray spot size of 2 mm²) in the Beamline 20A1, NSRRC, Taiwan. Each sample had three to four scans, which were averaged during the data processes. The spectra were calibrated, baseline-corrected, and edge-step-normalized by using ATHENA software from DEMETER (or IFEFFIT) software package (CARS, University of Chicago).³¹

2.4.5. ATR-FTIR Analysis. Functional groups of minerals and/or organic groups in the samples (including freeze-dried and powdered bulk tailing samples and powdered air-dried WSA samples) were determined by attenuated total reflection Fourier transform infrared (ATR-FTIR) using a Cary 630 FTIR (Agilent Technologies, Palo Alto, CA, USA). Spectra were collected between 400 and 4000 cm⁻¹ with a resolution of 2 cm⁻¹, totaling 64 scans. ATR-FTIR spectra of the tailing samples were processed by MicroLab software package and Origin 8.5 (OriginLab Corporation, Northampton, MA, USA).

2.4.6. NanoSIMS Analysis. The air-dried water-stable microaggregates were dispersed into the Milli-Q water (1:10)

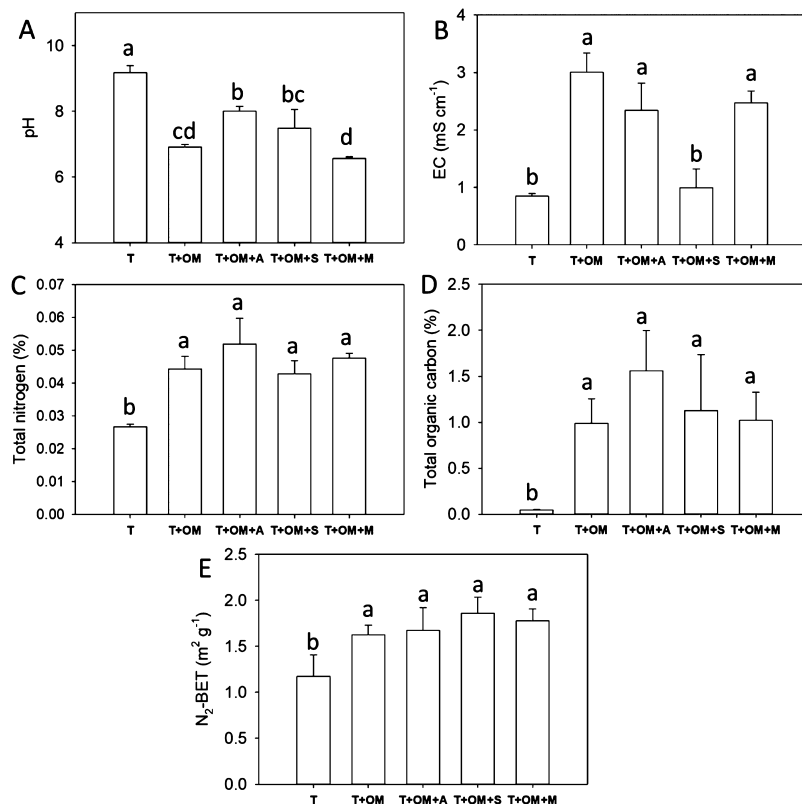


Figure 1. Basic physicochemical properties, including pH and EC, TOC, TN concentrations, and SSA (N_2 -BET) in tailings of different treatments. Different letters above the columns show significant difference among different treatments by Tukey's test ($P < 0.05$). Note: "T" represents tailings without any amendment, plus 4 month incubation; "T + OM" represents tailings amended with 3% w/w OM, plus 4 month incubation; "T + OM + A" represents tailings amended with 3% w/w OM, plus 2 month incubation, and additional 2 month colonization of *Acacia ramulosa*; "T + OM + S" represents tailings amended with 3% w/w OM, plus 2 month incubation, and additional 2 month colonization of *Sorghum* spp. Hybrid cv. Silk; and "T + OM + M" represents tailings amended with 3% w/w OM, plus 2 month incubation, and additional 2 month colonization of *Maireana brevifolia*.

and gently shaken (to remove inorganic CO_3^{2-}) according to Kopittke et al. (2017).³² Large quartz-like particles were allowed to settle, 0.1 mL of the suspension (containing the free organo-mineral association) was dropped onto a silica wafer, and the samples were dried in a desiccator for NanoSIMS analysis. Prior to NanoSIMS analysis, the samples were sputter-coated by Au to avoid charging during the measurements. In situ isotopic mapping was done by using NanoSIMS 50L (Cameca, Gennevilliers, France) located at the Centre for Microscopy, Characterisation and Analysis, University of Western Australia. See detailed information of NanoSIMS analysis in the Supporting Information.

2.5. Statistical Analysis. The significant differences in physicochemical characteristics and WSA percentage among the treatments were assessed by one-way analysis of variance ($P < 0.05$) followed with Tukey's test ($P < 0.05$) by using SPSS software package (Ver 18, IBM, Armonk, NY, USA).

3. RESULTS AND DISCUSSION

3.1. Tailing Neutralization and Aggregation Driven by OM Amendment and Plant Colonization. The present findings have confirmed our assumption that the OM amendment and plant colonization significantly improved the physicochemical properties of tailings, including neutralized alkaline pH conditions, increased TOC and TN levels, and elevated proportions of WSAs. The OM amendment and plant colonization neutralized tailing pH from the strongly alkaline

(>9) to circumneutral (i.e., around 7.5) (Figure 1A). This may have resulted from the effects of organic acids produced in microbial-mediated OM decomposition^{26,33} and also possibly from the exudates of plant roots.³³ After initial pH reduction in OM-amended tailings, the colonization of *A. ramulosa* and/or *Sorghum* spp. Hybrid cv. Silk colonization slightly reverted tailing pH (to nearly 8), which might have resulted from the excretion of HCO_3^- or OH^- by roots due to excessive uptake of anions over cations.³⁴ OM amendment prior to plant cultivation significantly increased EC value from below 1 mS cm^{-1} to above 3 mS cm^{-1} , likely resulting from the dissolution of abundant elements (e.g., K, Fe, Si, and Al) during the weathering of the primary minerals driven by microbial decomposition of added OM. In contrast, the colonization of plants (especially *Sorghum* spp. Hybrid cv. Silk) decreased the EC value (Figure 1B, $P < 0.05$), possibly because of the uptake of those dissolved/bioavailable elements by *Sorghum* spp. Hybrid cv. Silk roots. This was partially confirmed by the high concentrations of K, Ca, Mg, and Fe in plant tissues of *Sorghum* spp. (Table S2).²⁰

Both OM amendment and plant colonization significantly increased TN (Figure 1C) and TOC contents (Figure 1D), which resulted from the combined effects of added OM and their decomposed products, and/or from the plant root and their derived exudates. Most importantly, the OM and plant root interactions modified the surfaces of mineral particles and resulted in significant increases of N_2 -BET SSA in the treated

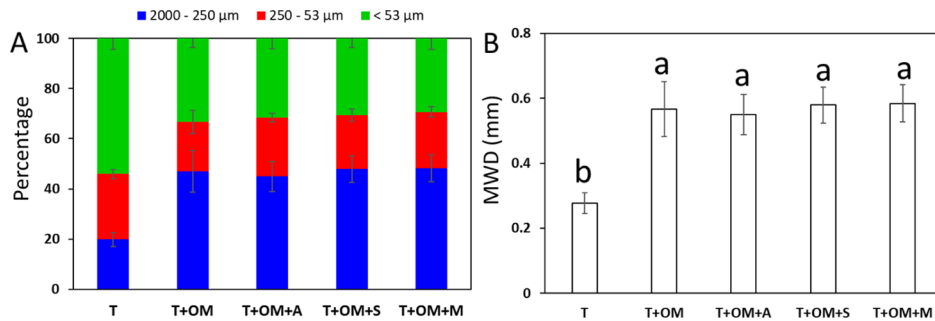


Figure 2. Percentage of water-stable aggregates (WSA) (A) and MWD (B) of tailings of different treatments. Different letters above columns show significant difference among different treatments by Tukey' test ($P < 0.05$). Note: “T”, “T + OM”, “T + OM + A”, “T + OM + S”, and “T + OM + M” are treatments labeled in Figure 1.

tailings (Figure 1E, $P < 0.05$). The increased SSA value of the tailings may have resulted from the weathering of primary minerals (i.e., biotite-like) into secondary phyllosilicate minerals (such as vermiculite and smectite groups), which possess higher SSA value compared with primary minerals.³⁵ This was consistent with the report from Wierzchos and Ascaso (1998)³⁶ showing that biotite was weathered through potassium loss and transformed to vermiculite induced by the activities of lichen. These changes are precursors favoring organo-mineral association and aggregate formation in the tailings.³⁷

OM amendment and plant colonization significantly increased percentage of macroaggregates from 20 to nearly 50% ($P < 0.05$, Figure 2A). The MWD value in tailings with OM and plant colonization treatment was around 0.55 mm, which was nearly two times of that in the control tailings (Figure 2B). Besides, more than 90% of the fractions above 0.25 mm in the tailings without OM and plant colonization treatment was quartz sands or small/fine fragments of mica, while the main fractions above 250 μm in the tailings subject to the OM and plant cultivation was mainly composed of “true” aggregates (tailing particles aggregated together) (Figure S3). The effects of different pioneer plants were similar on water-stable aggregate development, indicating the similar functionality of different plants toward tailing aggregation in the present study, although the specific processes may vary among them.³⁸ The water-stable aggregation enhanced by OM amendment and plant colonization may have been resulted from the integrated processes of (1) the bioweathering of the primary Fe-bearing minerals (especially biotite-like mica) and the formation of secondary Fe-/Si-/Al-rich minerals³⁹ and (2) secondary phyllosilicates and/or secondary Fe (oxy)hydroxides interact with OM to form organo-mineral association for water-stable aggregation.⁴⁰ Further detailed examination of Fe-bearing mineralogy and organo-mineral interactions have supported our expectations here.

3.2. Accelerated Weathering of Fe-Bearing Primary Minerals in the Tailings. 3.2.1. Altered XRD Patterns Revealed the Transformation of Primary Minerals in Tailings. The general XRD patterns in the tailings of different treatments were similar, with the dominant components of quartz, mica, pyroxene, amphibole, magnesioferrite, and minor amount of phases from ferrous oxide or illite (Figure 3). Specifically, analcime was found in the control tailings, which was a primary mineral commonly present in alkaline rocks.⁴¹ However, when tailings were treated with OM amendment and plant cultivation, analcime disappeared, suggesting the weathering and transformation of this primary silicate mineral into

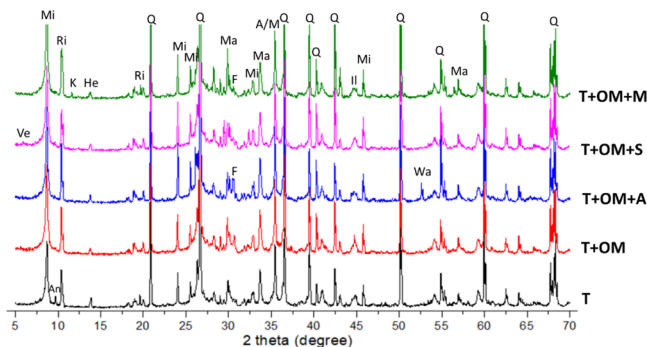


Figure 3. XRD spectra of tailings of different treatments. Note: Q: quartz; F: ferrous oxide; A: allophane ($\text{Al}_2\text{O}_3\cdot(\text{SiO}_2)_{1.3-2}\cdot(2.5-3)\text{H}_2\text{O}$); M: magnetite; Mi: mica, such as muscovite ($\text{Al}_{2.908}\text{H}_{0.12}\text{K}_{10}\text{Si}_{3.092}$), biotite ($\text{K}(\text{Mg},\text{Fe})_3(\text{AlSi}_3\text{O}_{10})(\text{F},\text{OH})_2$), phlogopite ($\text{KMg}_3(\text{AlSi}_3\text{O}_{10})(\text{F},\text{OH})_2$), annite ($\text{KFe}_3^{2+}\text{AlSi}_3\text{O}_{10}(\text{OH})_2$), etc.; An: analcime ($\text{NaAlSi}_2\text{O}_6\cdot\text{H}_2\text{O}$), usually classified as a zeolite mineral, a primary mineral in alkaline igneous rocks; Ve: vermiculite ($\text{Mg}_{0.7}(\text{Mg},\text{Fe},\text{Al})_6(\text{Si},\text{Al})_8\text{O}_{20}(\text{OH})_4\cdot8\text{H}_2\text{O}$); K: kaolinite ($\text{Al}_2\text{Si}_2\text{O}_5(\text{OH})_4$); Wa: wairakite, zeolite mineral ($\text{Ca}_8(\text{Al}_{16}\text{Si}_{32}\text{O}_{96})\cdot16\text{H}_2\text{O}$); He: hedenbergite ($\text{CaFeSi}_2\text{O}_6$), the iron-rich member of the pyroxene group; Ri: richterite ($(\text{Na},\text{K})_2(\text{Mg},\text{Mn},\text{Ca})_6\text{Si}_8\text{O}_{22}(\text{OH})_2$), belongs to amphibole group; Ma: magnesioferrite ($\text{Mg}(\text{Fe}^{3+})_2\text{O}_4$); Il: illite, ($\text{K}_0\text{H}_3\text{O})\cdot(\text{Al},\text{Mg},\text{Fe})_2(\text{Si},\text{Al})_4\text{O}_{10}[(\text{OH})_2, (\text{H}_2\text{O})]$). Note: “T”, “T + OM”, “T + OM + A”, “T + OM + S”, and “T + OM + M” are treatments labeled in Figure 1.

other minerals. At the same time, in the treatment with OM amendment and *Sorghum* spp. Hybrid cv. Silk colonization (i.e., “T + OM + S”), a small peak was observed at around $2\theta = 6.2^\circ$, as being further confirmed by the later XRD spectra of tailing aggregates from “T + OM + S” treatment. This indicated the formation of vermiculite (2:1-type clay minerals). In addition, kaolinite (1:1-type clay minerals) was also found in tailings treated with OM amendment and *M. brevifolia* colonization (i.e., “T + OM + M”), and some wairakite (zeolite mineral) occurred in tailings with OM amendment and *A. ramulosa* colonization (i.e., “T + OM + A”) (Figure 3).

The early vermiculitization (and/or kaolinization) of the biotite-like minerals in the tailings treated with OM and plant (*Sorghum* spp. Hybrid cv. Silk and *M. brevifolia*) colonization indicates that biotite-like minerals were undergoing weathering driven by the added root activities. The LMWOAs (including mainly citric acid, acetic acid, and oxalic acid, identified in our pre-experiment, Figure S4) from plant roots and continual microbial OM decomposition in the tailings may have facilitated biotite-like mineral weathering via ligand-promoted

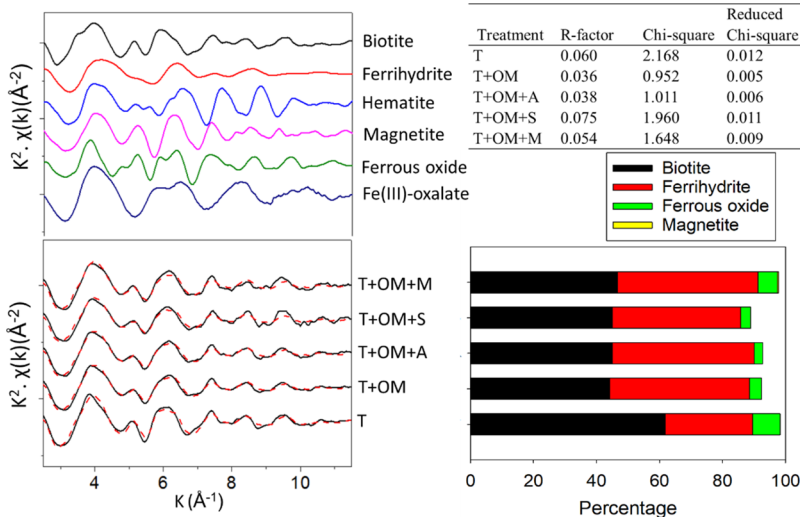


Figure 4. k space Fe K edge EXAFS spectra (line) and LCF (dashed) highlight the distinct Fe-bearing phases within the fresh tailings of different treatments. Fe K edge EXAFS spectra of several key Fe standards are also shown, including biotite, ferrihydrite, hematite, magnetite, ferrous oxide, and Fe(III)-oxalate. The right column shows the results of the LCF fitting of Fe K edge EXAFS spectra of tailings from different treatments. The parameters for the fittings are shown in the table above the column. Note: “T”, “T + OM”, “T + OM + A”, “T + OM + S”, and “T + OM + M” are treatments labeled in Figure 1.

pathway.⁴² The formation of vermiculite may have resulted from layer-by-layer transformation in the early stage of weathering of biotite.⁴³ The formation of kaolinite may have resulted from the pseudomorphic (isomorphic and largely isovolumetric) alteration of biotite⁴⁴ or from the further weathering of vermiculite.⁴⁵ Plant roots varied on their functions toward secondary phyllosilicate production, probably because of their different biochemical functions such as excreting exudates. For instance, the *Sorghum* spp. Hybrid cv. Silk is a species with phytosiderophore-assisted Fe-acquisition strategy and siderophores have high affinity to Fe and facilitate Fe dissolution from the primary minerals,⁴⁶ while the other two plant species tested here did not have such exudates.

3.2.2. Mineral Weathering and Fe Speciation as Revealed by Fe K Edge XAFS. Cryo-Fe K edge XAFS analysis revealed different Fe speciations in the fresh tailings of the treatments (Figures 4, S5 and S6). The intensity of the Fe K edge XANES peak at around 7130 eV in tailings decreased upon OM amendment and plant colonization treatment. The OM with *Sorghum* spp. Hybrid cv. Silk colonization (treatment “T + OM + S”) had the lowest intensity at around 7130 eV (Figure SSA). Further LC-XANES fitting indicated that biotite-like minerals decreased while ferrihydrite-like components increased in the tailings after OM and plant colonization treatment (Figure S6), which was confirmed by further LC-EXAFS fitting (Figure 4). Moreover, some Fe(III)-oxalate analogues started to appear in the tailings after *M. brevifolia* colonization (“T + OM + M”, Figure S6). These results confirmed that the biotite-like minerals were undergoing weathering and transformation into secondary minerals including ferrihydrite-like minerals, and the presence of Fe(III)-oxalate analogues indicated that the weathering processes might be stimulated by ligand-promoted pathway as mentioned above.⁴² The identified FeO-like minerals may have resulted from Fe²⁺ containing phyllosilicates (such as biotite, amphibole, olivine, etc.).^{47,48} It is essential to note that in the LC-XANES and EXAFS fitting, the sum of components was not 100%, indicating that there might be other Fe species present but not identified in the fitting. Besides, it is worth

pointing out here that XANES is performed mainly on low- k (less than 2.5 in the k space) near the absorption edge (−20 to 30 eV), and more sensitive at oxidation state and coordination chemistry, while EXAFS is more on high k (above 2.5 in the k space) with 30–800 eV in the postedge, and more sensitive to the photoelectrons scattering and interactions between the core element and their neighbor atoms.⁴⁹ Therefore, we found that the linear combination fitting (LCF) analysis of XANES and EXAFS revealed different profiles of findings with the Fe-bearing minerals.

The Fe atomic structure changes were also investigated by FT-EXAFS analysis, which showed generally two main shells of Fe core. Tailings with different treatments had a similar peak position and intensity in the first shell (Figure SSB). However, in the second shell, the tailings after OM amendment and *Sorghum* spp. Hybrid cv. Silk (and/or *M. brevifolia*) colonization had higher amplitude than the other treatments (Figure SSB). Specifically, the number of Fe–Fe interatomic distances at 3.07–3.14 Å decreased after OM and plant colonization treatments (Table S3, Figure SSC). However, the tailings in treatments “T + OM + S” and “T + OM + M” had more Al/Si atoms around Fe at a distance of 3.31–3.36 Å than the tailings in other treatments. These may have suggested that the Fe atomic environment and their association with possible Al and/or Si may have been altered in the rhizosphere tailings during the weathering of primary minerals and formation of new mineral phases. It is essential to point out that the shell-by-shell fitting of Fe K edge EXAFS spectra in samples with multiple Fe mineral phases is not fully reliable, as various elements at different distances could have collectively contributed to single atomic Fe neighbors, and their features could not be accurately modeled in the present situation. Therefore, these results should be considered properly, together with the results of other analysis (e.g., LC-XANES, LC-EXAFS, XRD, and ATR-FTIR).

3.2.3. Weathering Induced Morphological Changes of Fe-Bearing Minerals As Revealed by BSE-SEM-EDS. In the control tailings (treatment “T”), Fe–Si–K-rich primary minerals observed under SEM-EDS should be attributed to

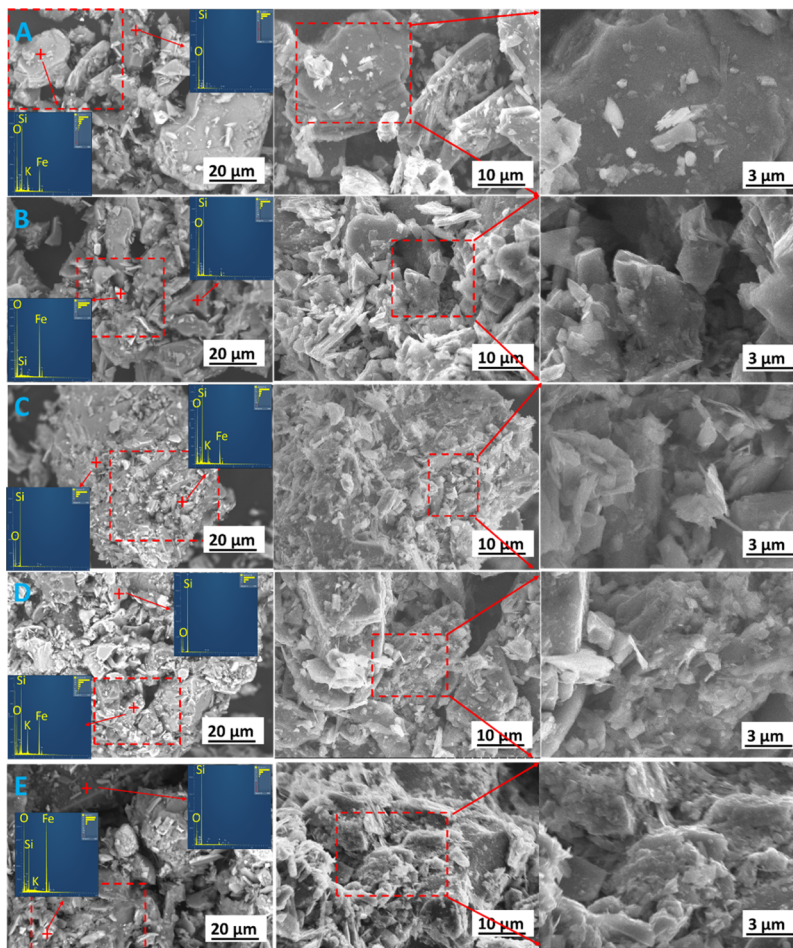


Figure 5. BSE-SEM-EDS showing morphology and elemental composition of Fe-bearing minerals in tailings of different treatments. (A) “T”; (B) “T + OM”; (C) “T + OM + A”; (D) “T + OM + S”; and (E) “T + OM + M”. The right ones are magnified rectangle areas in the left ones. Note: “T”, “T + OM”, “T + OM + A”, “T + OM + S”, and “T + OM + M” are treatments labeled in Figure 1.

biotite-like mica, as revealed by both XRD and Fe K edge XAFS analysis (Figure 5A). Big particles with Fe-rich minerals with smooth surface were broken into small particles exhibiting a certain amount of irregularly shaped minerals on the surfaces of the tailing particles, in treatments of OM amendment and plant colonization (Figure 5B). Especially, compared with the tailings treated only with OM (“T + OM”), the plant colonization tended to accelerate the biow weathering processes, resulting in increased small-size irregular Fe-rich minerals in the tailings of treatments “T + OM + A”, “T + OM + S”, and “T + OM + M” (Figure 5). By further examination under cryo-SEM, irregular Fe-/Si-/Al-rich minerals were observed on the surface of the tailing minerals, which were most likely the weathering products deposited on the surface (Figure S7). In addition, some areas in the tailings from OM and plant treatments only consisted of Fe and O with much low amount of Si (Figure 5B), confirming the Fe (oxy)hydroxides revealed by the Fe K edge XAFS analysis. Increased amounts of Fe (oxy)hydroxides such as ferrihydrite analogues were formed during Fe-bearing mineral weathering driven by OM addition and plant colonization.⁵⁰ The formation of secondary minerals on tailing surface indicated that the weathering of tailing minerals was at its initial stage, which could be due to ligand-promoted dissolution of primary minerals⁴² driven by LMWOAs (Figure S4) derived from plant root exudates and OM decomposition products.²⁶ Nevertheless, roles of physical

force from plant roots and rhizosphere microbes (such as fungal mycelium) cannot be excluded from the total effects on the mineral weathering.¹⁷ The resultant effects of these initial weathering of primary minerals in the tailings in OM and plant colonization treatments led to increased surface area (i.e., increased SSA, Figure 1E) of the minerals favoring organo-mineral interactions and aggregate formation.

3.3. Mineral and Organic Functional Groups Favoring Aggregation in Tailings Modified by OM Amendment and Plant Colonization. In the ATR-FTIR spectra of tailings with different treatments, the main peaks in all the tailing samples appeared at 941 cm⁻¹ (Figure S8A), which represented the OH deformation of inner-surface hydroxyl groups.⁵¹ The area of the peaks at this position decreased upon OM and plant treatment, indicating the involvement of inner surface OH in the organo-mineral or mineral–mineral interactions. The peaks at 776, 799, and 692 cm⁻¹, as well as at 950–1115 cm⁻¹, were observed in the tailings across all treatments, which represented Si–O stretching of quartz, phyllosilicates, and/or silica.⁵¹ All tailing samples of the treatments exhibited peaks at 3533 and 3356 cm⁻¹ (Figure S8B), indicating OH stretching of water coordinated to Al or Mg.⁵¹ The peaks at 1634 cm⁻¹ in tailings of OM and plant colonization treatments suggested the presence of aromatic C stretching or asymmetric C–O stretching of carboxyl groups.⁵² Besides, peaks at 1433 cm⁻¹ appeared in tailings of OM and

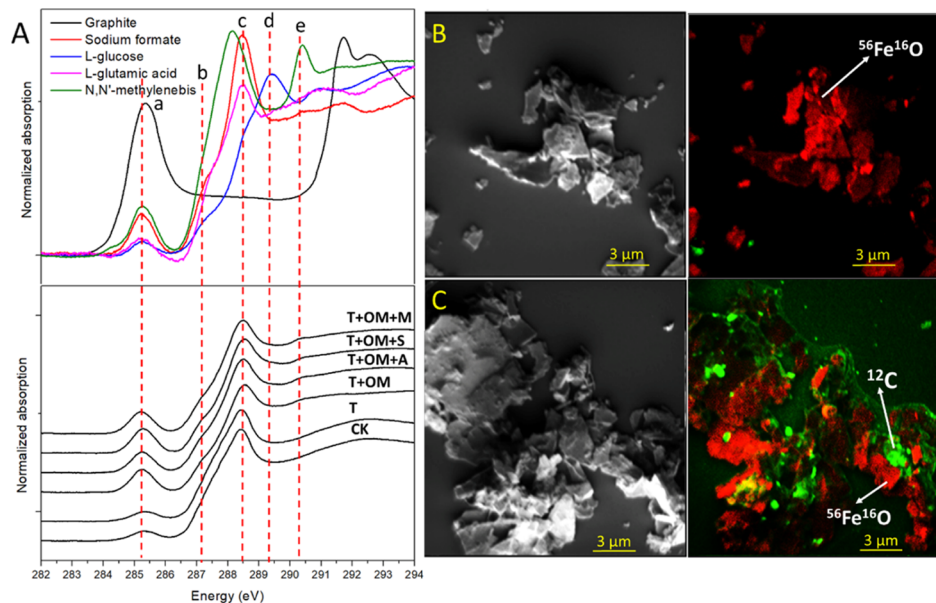


Figure 6. (A) Synchrotron-based C 1s NEXAFS spectra of tailing microaggregates (water-stable) from different treatments. The C 1s NEXAFS spectra of organic C standards including graphite (solely aromatic C), L-glucose (solely O–alkyl C), Na formate (solely carboxyl C), L-glutamic acid (alkyl C, carboxyl C), and N,N'-methylenebis (acrylamide) (rich in carbonyl C) are also shown for verifying the peaks of organic C forms. Note: a, 285.2 eV, aromatic C; b, 287.1 eV, alkyl C; c, 288.5 eV, carboxyl C; d, 289.3 eV, O–alkyl C; e, 290.3 eV, carbonyl C. (B,C) Two-dimensional NanoSIMS images showing distribution of ^{12}C and $^{56}\text{Fe}^{16}\text{O}$ in the control tailing particles (B), and tailing aggregates after OM treatment (C). In (B,C), the left image is the contrast image showing tailing minerals, the right dicolor map shows the relationship between Fe-rich minerals and organic C, the red is $^{56}\text{Fe}^{16}\text{O}$ (counts range: 0–335), and the green one is ^{12}C (counts range: 0–100). Note: “CK” is the control sample holder without samples; “T”, “T + OM”, “T + OM + A”, “T + OM + S”, and “T + OM + M” are treatments labeled in Figure 1.

plant treatment (Figure S8B), which might represent the deformation of OH from carboxylic structures.⁵³ It was noted that a peak at 1433 cm^{-1} was also found in the control tailings (with less than 0.1% organic C content), which might be the ammonium or carbonate that could adsorb radiation at 1420 – 1440 cm^{-1} .^{53,54} This is reasonable, as the untreated tailings were strongly alkaline, which may have stabilized a certain amount of ammonium and/or carbonate. The increased carboxyl (and/or aromatic) groups in tailings of OM and plant treatment were logically attributed to the decomposition of OM (i.e., sugarcane mulch in the present study) and plant root activities. These functional organic groups in organics readily interact with minerals via ligand-exchange reactions,⁵⁵ and/or via hydrophobic absorption by minerals,⁵⁶ leading to organo-mineral association and formation of WSAs in the tailings.

3.4. Functional Organic Groups and Secondary Fe-Bearing Minerals Support WSA Formation in the Tailings. **3.4.1. Organic Groups as Aggregate Cements via Complexation with Fe-Bearing Minerals.** Macro- and micro-aggregates isolated from the tailings of OM and plant colonization treatments exhibited FTIR peaks at 1634 and 1433 cm^{-1} representing aromatic C=C stretching and asymmetric C–O stretching of carboxyl groups,⁵² as well as the deformation of OH from carboxylic structures,⁵³ which were hardly found in control tailing macroparticles ($>250\text{ }\mu\text{m}$), and discrete particles (Figure S8C–F). The C 1s NEXAFS further revealed that the tailing microaggregates contained aromatic C (285.2 eV), alkyl C (287.1 eV), carboxyl C (288.5 eV), and carbonyl C (290.3 eV), which were found to be negligible in the control tailing particles (Figure 6A), indicating that those organic functional groups may participate in organo-mineral association for aggregation. There also appears a peak

at 288.5 eV in tailing particles (“T”), which may not be real carboxyl C, as the peak shape was different from that of the tailing aggregates with OM and plant treatments, and more like the peaks produced in the control (empty) sample holder (“CK”). It was also notable that the peaks at 285.2, 287.1, 289.3, and 290.3 eV were not completely absent in “CK” and “T”, which might be due to the tiny impurity containing organic groups in the sample holder. The C 1s NEXAFS analysis further confirmed ATR–FTIR results, showing that the aggregates of tailings contained aromatic C, carboxyl C, and aliphatic C (rich in alkyl C) and carbonyl C after OM and plant cultivation treatments. These organic groups (especially those rich in oxygen, such as carbonyl C and carboxyl C) would have great potential to readily interact with minerals,^{10,57} acting as persistent binding/bridging agents⁵⁸ for aggregate formation.

Because there was no significant difference in WSA distribution and organic carbon forms between those treatments with OM and plant cultivation, we selected water-stable microaggregate samples from the treatment “T + OM” as a representative for in situ examination of organic C localization and their association with Fe-bearing minerals, by employing NanoSIMS. The control tailing particles without OM and plant treatments was also tested for comparison. As revealed by NanoSIMS analysis, organic carbon was barely detected in the control tailings without eco-engineering input (Figure 6B). In contrast, after being treated with OM, the organic C was detected within the tailing microaggregates (Figure 6C), which were heterogeneously distributed on the surface of Fe-rich minerals, forming organo-Fe-bearing mineral associations. This pattern of organic C distribution was consistent with soil aggregates investigated by Lehmann et al. (2008)⁵⁹ who observed that soil organic C was present at “distinct locations

Table 1. Results of LCF of Fe K Edge XANES Spectra of WSAs of Different Sizes from Tailings of Different Treatments^a

	aggregate size	biotite	ferrihydrite	ferrous oxide	illite	Fe(III)-oxalate	R factor	chi-square	reduced Chi-square
T + OM	macroaggregate	50.8	39.9	10.0	0	0	0.00044	0.01517	0.00012
	microaggregate	48.9	40.3	11.5	0	0	0.00046	0.01612	0.00013
	discrete particles	53.8	39.7	5.6	1.6	0	0.00047	0.01667	0.00014
T + OM + A	macroaggregate	62.1	26.5	2.0	0	11.1	0.00043	0.01588	0.00013
	microaggregate	55.4	22.3	0	12.4	10.3	0.00044	0.01669	0.00014
	discrete particles	52.5	40.7	6.7	0	0.7	0.00043	0.01490	0.00012
T + OM + S	macroaggregate	57.4	30.2	5.8	0	8.0	0.00044	0.01608	0.00013
	microaggregate	61.1	33.0	0	1.3	6.9	0.00047	0.01748	0.00014
	discrete particles	52.5	39.0	6.9	0	2.7	0.00041	0.01466	0.00012
T + OM + M	macroaggregate	56.2	26.5	9.4	0	9.0	0.00062	0.02213	0.00018
	microaggregate	61.8	18.4	5.5	0	17.4	0.00056	0.02124	0.00017
	discrete particles	51.0	37.5	11.4	1.1	0	0.00054	0.01909	0.00016

^a"T + OM" represents tailings amended with 3% w/w OM, plus 4 month incubation; "T + OM + A" represents tailings amended with 3% w/w sugarcane mulch, plus 2 month incubation, and additional 2 month colonization of *Acacia ramulosa*; "T + OM + S" represents tailings amended with 3% w/w sugarcane mulch, plus 2 month incubation, and additional 2 month colonization of *Sorghum* spp. Hybrid cv. Silk; and "T + OM + M" represents tailings amended with 3% w/w sugarcane mulch, plus 2 month incubation, and additional 2 month colonization of *Maireana brevifolia*.

of the mineral assemblage." Particle size of Fe-rich minerals that associated with organic C ranged from nearly 1 μm in diameter to 10 μm . Furthermore, we found that some small mineral particles (diameter ca. 3 μm) rich in Fe and Al could also sequestrate organic C on the surface of the minerals (Figure S9). Those Fe-/Al-rich minerals should possibly be Fe-bearing phyllosilicates (such as biotite-like minerals and/or their weathered products), which may have participated in the sequestration of organic C. The NanoSIMS findings provided solid evidence of organic C interactions with Fe-rich minerals within tailing aggregates, supporting our assumptions that the interactions between organic carbon and Fe-rich minerals would contribute to the WSA formation in the tailings.

Furthermore, as indicated by Fe K edge XANES analysis, the Fe(III)-oxalate complex (3.6–17.4%) was potentially present in the aggregates of tailings with OM and plant treatments but not in the discrete particles (Table 1, Figure S10). This was partially consistent with the further shell-by-shell fitting of Fe K edge EXAFS spectra, which indicated the possible presence of Fe–C distances at 2.59–2.68 Å in tailing aggregates of treatments "T + OM + A" and "T + OM + M" (Table S4, Figure S11). These Fe(III)-carboxyl complex analogues as key constituents of the aggregates may have been formed in the interactions of dissolved Fe ions or amorphous Fe minerals with carboxyl groups (as revealed by both ATR–FTIR and C 1s NEXAFS analysis) via ligand exchange.^{13,55} Further LCF analysis of EXAFS spectra confirmed that the key Fe components in the WSAs from different treatments were ferrihydrite (ca. 50%) and biotite (ca. 40%) (Figure S12, Table S5). The ferrihydrite possessed a high adsorption capacity for organic molecules/ligands because of their abundant surface Fe–OH groups.⁶⁰ In addition, the bioweathering of biotite-like mica in the tailings resulted in the deposition of some secondary phyllosilicates such as vermiculite or kaolinite (revealed by XRD analysis, Figures 3 and S13), which could have also complexed with organic functional groups via surface complexation reactions at their active surface OH sites (e.g., Al–OH).⁶¹ It is important to point out that some hydrophobic substances rich in aromatic C (and/or big aliphatic chain) could have also been absorbed on the surfaces of minerals via hydrophobic interactions⁵⁶ and act as cementation agents for aggregation.⁶² These interactions between organic functional groups and Fe-bearing secondary minerals (both hydrophilic

and hydrophobic interactions) would have further contributed to the water-stable aggregation.

3.4.2. Secondary Fe-Bearing Minerals as Aggregate Cements. In addition to the role of organic cements, the interactions of Fe (oxy)hydroxides with Si/Al hydroxides via possibly substitution reactions may lead to the formation of possible Fe–Al/Si-rich gel minerals.^{9,63} BSE-SEM-EDS analysis revealed small irregular Fe–Si-rich gel-like minerals in tailings treated with OM and plant colonization (Figures 5 and S7). Especially, BSE-SEM-EDS analysis of the polished tailing aggregates (e.g., aggregates from treatment "T + OM + S") showed that the quartz and mica particles were connected by those small-size Fe (oxy)hydroxides (contained mainly Fe and O) and/or Fe–Si–Al-rich irregular and spherical minerals (revealed by EDS) (Figure S14). Besides, the shell-by-shell fitting of Fe K edge EXAFS spectra also indicated the increase of Al/Si atoms around Fe at a distance of 3.29–3.35 Å in the tailings after being treated with OM amendment and plant colonization (including *Sorghum* spp. Hybrid cv. Silk and *M. brevifolia*) (Table S3). This may partially indicate the presence of Fe–Si–Al-rich mineral gels. These gels may glue quartz and mica particles together, playing critical roles in the formation of WSAs in the tailings.⁹

3.4.3. Inner-Surface Hydroxyl Groups as Key Reaction Sites. As mentioned above, the ATR–FTIR peaks at 941 cm⁻¹ (represents deformation of inner surface OH groups) in tailings decreased significantly after OM and plant colonization (Figure S8A). The inner-surface OH groups may be located in phyllosilicates (both primary and secondary Fe-rich aluminosilicates such as biotite⁶⁴) and/or Fe (oxy)hydroxides (e.g., ferrihydrite)⁶⁵ in the tailings. Despite the fact that the OM amendment and plant colonization stimulated the weathering of primary minerals in the tailings, the decreased density of OH groups in tailing minerals was contrary to our expectation. This was most likely because the majority of surface OH groups in minerals may have reacted with organic functional groups (such as carboxyl/aromatic groups) via ligand exchange in the tailings with OM amendment and plant colonization treatments (at circumneutral and slightly alkaline pH).⁶¹ Besides, the surface OH groups may also be involved in the interactions between Fe (oxy)hydroxides and phyllosilicates, as positively charged Fe–OH on Fe (oxy)hydroxide surface could readily interact with negatively charged basal plates of

phylosilicates.⁶⁶ In addition, the decreased OH in the tailings after OM and plant treatment may also indirectly favor the coating of hydrophobic OM on the mineral surface, as high density of OH usually facilitates water molecules binding to the minerals and increases hydrophilicity.⁶⁷ Furthermore, the peak area at around 941 cm⁻¹ in microaggregates was much lower than that in macroaggregates or discrete particles (Figure S15), confirming that the inner-surface OH groups in minerals may be involved in organo-mineral interactions or mineral–mineral interactions especially in microaggregates, which were more stable than macroaggregates.⁶⁸ The lower amount of OH in microaggregate may also favor hydrophobic interactions between large organic groups and Fe-bearing minerals, contributing to the aggregate stability.

It is essential to point out that alkaline pH conditions of tailings could influence organo-mineral association or mineral–mineral association.⁶⁹ Fe (oxy)hydroxides usually contain variable charges depending on the surface of Fe–OH sites, while Fe-bearing phyllosilicates usually carry permanent negative charges on the basal plane resulting from isomorphic substitution of Al/Si ions in the crystal lattice with lower positive valence ions, as well as variable surface charge based on the surface Al/Si–OH sites.⁶¹ With the pH decreased from alkaline (pH 9.5) to circumneutral (pH 7.5) in the tailings after OM amendment and plant colonization, some of the Fe (oxy)hydroxides or phyllosilicates would have been positively charged on the surface,⁶¹ thus facilitating adsorption (electrostatic interactions) and/or complexation of negatively charged organic functional groups (carboxyl groups) on the surface of Fe (oxy)hydroxides and/or phyllosilicates. In addition, those unweathered biotite-like primary minerals may become positively charged with decreasing pH below their points of zero charge⁷⁰ and further enhanced the uptake of negatively charged OM.⁶¹

3.5. Environmental Implications. The present study has been the first to have unraveled at microscale that OM amendment and plant colonization initiated and accelerated soil structure formation in alkaline, finely textured, and mechanically compacted magnetite Fe ore tailings. Especially, OM amendment together with plant colonization facilitated water-stable aggregation via enhancing the weathering of primary Fe-bearing minerals (mainly biotite-like minerals), the formation of secondary Fe–Si-rich mineral gels, and the interactions of secondary minerals with organic groups (such as carboxyl and/or aromatic groups). These findings supported our concept that the Fe ore tailings rich in primary minerals (but lack of heavy metal contamination) may be eco-engineered into soil-like structure by low amount of OM input and pioneer plant colonization for sustainable tailing site rehabilitation.¹ The signatures found in the study (i.e., surface mineral weathering, organic carbon sequestration by Fe-rich minerals, and WSA formation) underpin our confidence in further developing the methodology for eco-engineering tailings into soils by utilizing sustainable resources of native pioneer plants and biomass–OM in the field. In addition, the present findings have also added new knowledge of organic C sequestration at least, during the initial pedogenesis of Fe ore mine tailings. As far as we have known, the organic C sequestration has been intensively studied in the nature soil system, in response to the climate change and soil management practices,⁷¹ but less information has been available for the potential role of organic C sequestration in initial soil aggregate structure formation in lithosphere Fe ore minerals. The present

findings have filled this knowledge gap about mineral weathering coupled with functional organic C sequestration (with Fe-rich minerals) in Fe ore tailings, contributing to the understanding of relationship between Fe-rich mineral mediated organic C sequestration and eco-engineered pedogenesis in Fe ore minerals.

ASSOCIATED CONTENT

Supporting Information

The Supporting Information is available free of charge on the ACS Publications website at DOI: 10.1021/acs.est.9b04526.

Diagram of experimental design and data of plant biomass and elemental concentrations, Fe K edge XAFS fitting results, and results of cryo-SEM/BSE-SEM-EDS, XRD, ATR–FTIR, and NanoSIMS, as well as photos showing wet-sieving (PDF)

AUTHOR INFORMATION

Corresponding Author

*E-mail: l.huang@uq.edu.au. Phone: +61 7 3346 3130. Fax: +61 7 3346 4056.

ORCID

Songlin Wu: 0000-0001-7469-5253

Tuan A. H. Nguyen: 0000-0002-3024-2081

Longbin Huang: 0000-0001-5024-0107

Notes

The authors declare no competing financial interest.

ACKNOWLEDGMENTS

This work was financially supported by the Australia Research Council Linkage Project (ARC-LP 019806). S.W. also acknowledges the UQ-ECR funding (613767). The authors acknowledge the staffs in the Centre for Microscopy and Microanalysis, Australian Microscopy & Microanalysis Research Facility, The University of Queensland for assistance in cryo-SEM, XRD, and BSE-SEM-EDS analysis. Besides, the Queensland node of the Australian National Fabrication Facility (ANFF-Q) was also acknowledged for ATR–FTIR analysis. The authors thank L. Robertson, Q. Yi, M. Hall, F. You, N. Saha, Y. Zhang, F. Saavedra, and J. Xue for casual help on the experiments. The authors also thank the associate editor, Prof. Daniel Giammar, and three anonymous reviewers for their constructive comments and suggestions which significantly improved the manuscript.

REFERENCES

- (1) Wu, S.; Liu, Y.; Southam, G.; Robertson, L.; Chiu, T. H.; Cross, A. T.; Dixon, K. W.; Stevens, J. C.; Zhong, H.; Chan, T.-S.; Lu, Y.-J.; Huang, L. Geochemical and mineralogical constraints in iron ore tailings limit soil formation for direct phytostabilization. *Sci. Total Environ.* **2019**, *651*, 192–202.
- (2) Huang, L.; Baumgartl, T.; Mulligan, D. Is rhizosphere remediation sufficient for sustainable revegetation of mine tailings? *Ann. Bot.* **2012**, *110*, 223–238.
- (3) Huang, L.; Baumgartl, T.; Zhou, L.; Mulligan, D. The New Paradigm for Phytostabilising Mine Wastes—Ecologically Engineered Pedogenesis and Functional Root Zones. *Life-of-Mine* **2014**; AUSIMM, 2014; pp 663–674.
- (4) Wu, S.; Nguyen, T. A. H.; Liu, Y.; Southam, G.; Wang, S.; Chan, T.-S.; Lu, Y.-R.; Huang, L. Deficiencies of secondary Fe (oxy)hydroxides associated with phyllosilicates and organic carbon limit the formation of water-stable aggregates in Fe-ore tailings. *Chem. Geol.* **2019**, *S23*, 73–87.

- (5) Herrick, J. E.; Whitford, W. G.; De Soya, A. G.; Van Zee, J. W.; Havstad, K. M.; Seybold, C. A.; Walton, M. Field soil aggregate stability kit for soil quality and rangeland health evaluations. *Catena* **2001**, *44*, 27–35.
- (6) Regelink, I. C.; Stoof, C. R.; Rousseva, S.; Weng, L.; Lair, G. J.; Kram, P.; Nikolaidis, N. P.; Kercheva, M.; Banwart, S.; Comans, R. N. J. Linkages between aggregate formation, porosity and soil chemical properties. *Geoderma* **2015**, *247–248*, 24–37.
- (7) Amézketa, E. Soil aggregate stability: a review. *J. Sustain. Agric.* **1999**, *14*, 83–151.
- (8) Denef, K.; Six, J. Clay mineralogy determines the importance of biological versus abiotic processes for macroaggregate formation and stabilization. *Eurasian J. Soil Sci.* **2005**, *56*, 469–479.
- (9) Eggleton, R. A. Noncrystalline Fe-Si-Al-oxyhydroxides. *Clays Clay Miner.* **1987**, *35*, 29–37.
- (10) Coward, E. K.; Ohno, T.; Plante, A. F. Adsorption and molecular fractionation of dissolved organic matter on iron-bearing mineral matrices of varying crystallinity. *Environ. Sci. Technol.* **2018**, *S2*, 1036–1044.
- (11) Chenu, C.; Le Bissonnais, Y.; Arrouays, D. Organic matter influence on clay wettability and soil aggregate stability. *Soil Sci. Soc. Am. J.* **2000**, *64*, 1479–1486.
- (12) Yuan, M.; Xu, Z. P.; Baumgartl, T.; Huang, L. Organic Amendment and Plant Growth Improved Aggregation in Cu/Pb-Zn Tailings. *Soil Sci. Soc. Am. J.* **2016**, *80*, 27–37.
- (13) Kleber, M.; Sollins, P.; Sutton, R. A conceptual model of organo-mineral interactions in soils: self-assembly of organic molecular fragments into zonal structures on mineral surfaces. *Biogeochemistry* **2007**, *85*, 9–24.
- (14) Zanuzzi, A.; Arocena, J. M.; Van Mourik, J. M.; Faz Cano, A. Amendments with organic and industrial wastes stimulate soil formation in mine tailings as revealed by micromorphology. *Geoderma* **2009**, *154*, 69–75.
- (15) Angers, D. A.; Caron, J. Plant-induced changes in soil structure: processes and feedbacks. *Biogeochemistry* **1998**, *42*, 55–72.
- (16) Banfield, J. F.; Barker, W. W.; Welch, S. A.; Taunton, A. Biological impact on mineral dissolution: application of the lichen model to understanding mineral weathering in the rhizosphere. *Proc. Natl. Acad. Sci. U.S.A.* **1999**, *96*, 3404–3411.
- (17) Bonneville, S.; Morgan, D. J.; Schmalenberger, A.; Bray, A.; Brown, A.; Banwart, S. A.; Benning, L. G. Tree-mycorrhiza symbiosis accelerate mineral weathering: Evidences from nanometer-scale elemental fluxes at the hypha–mineral interface. *Geochim. Cosmochim. Acta* **2011**, *75*, 6988–7005.
- (18) Calvaruso, C.; Turpault, M.-P.; Frey-Klett, P. Root-associated bacteria contribute to mineral weathering and to mineral nutrition in trees: a budgeting analysis. *Appl. Environ. Microbiol.* **2006**, *72*, 1258–1266.
- (19) Nevill, P. G.; Wallace, M. J.; Miller, J. T.; Krauss, S. L. DNA barcoding for conservation, seed banking and ecological restoration of Acacia in the Midwest of Western Australia. *Mol. Ecol. Resour.* **2013**, *13*, 1033–1042.
- (20) Baum, S. F.; Tran, P. N.; Silk, W. K. Effects of salinity on xylem structure and water use in growing leaves of sorghum. *New Phytol.* **2000**, *146*, 119–127.
- (21) You, F.; Dalal, R.; Huang, L. Initiation of soil formation in weathered sulfidic Cu-Pb-Zn tailings under subtropical and semi-arid climatic conditions. *Chemosphere* **2018**, *204*, 318–326.
- (22) Noël, V.; Marchand, C.; Juillot, F.; Ona-Nguema, G.; Viollier, E.; Marakovic, G.; Olivi, L.; Delbes, L.; Gelebart, F.; Morin, G. EXAFS analysis of iron cycling in mangrove sediments downstream a lateritized ultramafic watershed (Vavoutou Bay, New Caledonia). *Geochim. Cosmochim. Acta* **2014**, *136*, 211–228.
- (23) Bardelli, F.; Barone, G.; Crupi, V.; Longo, F.; Maisano, G.; Majolino, D.; Mazzoleni, P.; Venuti, V. Iron speciation in ancient Attic pottery pigments: a non-destructive SR-XAS investigation. *J. Synchrotron Radiat.* **2012**, *19*, 782–788.
- (24) Wan, J.; Tyliszczak, T.; Tokunaga, T. K. Organic carbon distribution, speciation, and elemental correlations within soil microaggregates: applications of STXM and NEXAFS spectroscopy. *Geochim. Cosmochim. Acta* **2007**, *71*, 5439–5449.
- (25) Mueller, C. W.; Weber, P. K.; Kilburn, M. R.; Hoeschen, C.; Kleber, M.; Pett-Ridge, J. Advances in the analysis of biogeochemical interfaces: NanoSIMS to investigate soil microenvironments. In *Advances in Agronomy*; Academic Press, Elsevier, 2013; Vol. 121, pp 1–46.
- (26) You, F.; Zhang, L.; Ye, J.; Huang, L. Microbial decomposition of biomass residues mitigated hydrogeochemical dynamics in strongly alkaline bauxite residues. *Sci. Total Environ.* **2019**, *663*, 216–226.
- (27) Huang, C. Y. L.; Schulte, E. E. Digestion of plant tissue for analysis by ICP emission spectroscopy. *Commun. Soil Sci. Plant Anal.* **1985**, *16*, 943–958.
- (28) Kemper, W.; Rosenau, R. Aggregate stability and size distribution. In *Methods of Soil Analysis, Part 1: Physical and Mineralogical Methods*; Klute, A., Ed.; Soil Science Society of America: Madison, Wisconsin, USA, 1986; pp 425–442.
- (29) Peth, S.; Horn, R.; Beckmann, F.; Donath, T.; Fischer, J.; Smucker, A. J. M. Three-dimensional quantification of intra-aggregate pore-space features using synchrotron-radiation-based microtomography. *Soil Sci. Soc. Am. J.* **2008**, *72*, 897.
- (30) Steffens, M.; Rogge, D. M.; Mueller, C. W.; Höschen, C.; Lugmeier, J.; Kölbl, A.; Kögel-Knabner, I. Identification of distinct functional microstructural domains controlling c storage in soil. *Environ. Sci. Technol.* **2017**, *S1*, 12182–12189.
- (31) Ravel, B.; Newville, M. ATHENA, ARTEMIS, HEPHAESTUS: data analysis for X-ray absorption spectroscopy using IFEFFIT. *J. Synchrotron Radiat.* **2005**, *12*, 537–541.
- (32) Kopittke, P. M.; Hernandez-Soriano, M. C.; Dalal, R. C.; Finn, D.; Menzies, N. W.; Hoeschen, C.; Mueller, C. W. Nitrogen-rich microbial products provide new organo-mineral associations for the stabilization of soil organic matter. *Glob. Chang. Biol.* **2018**, *24*, 1762–1770.
- (33) Jones, D. L. Organic acids in the rhizosphere—a critical review. *Plant Soil* **1998**, *205*, 25–44.
- (34) Marschner, H. *Mineral Nutrition of Higher Plants*; Academic Press: Boston, MA, 1995.
- (35) Dogan, M.; Dogan, A. U.; Yesilyurt, F. I.; Alaygut, D.; Buckner, I.; Wurster, D. E. Baseline studies of the clay minerals society special clays: Specific surface area by the Brunauer–Emmett–Teller (BET) method. *Clays Clay Miner.* **2007**, *55*, 534–541.
- (36) Wierchos, J.; Ascaso, C. Mineralogical transformation of bioweathered granitic biotite, studied by HRTEM: evidence for a new pathway in lichen activity. *Clays Clay Miner.* **1998**, *46*, 446–452.
- (37) Eusterhues, K.; Rumpel, C.; Kögel-Knabner, I. Organo-mineral associations in sandy acid forest soils: importance of specific surface area, iron oxides and micropores. *Eur. J. Soil Sci.* **2005**, *56*, 753–763.
- (38) Garcia, C.; Roldan, A.; Hernandez, T. Ability of different plant species to promote microbiological processes in semiarid soil. *Geoderma* **2005**, *124*, 193–202.
- (39) Duiker, S. W.; Rhoton, F. E.; Torrent, J.; Smeek, N. E.; Lal, R. Iron (hydr) oxide crystallinity effects on soil aggregation. *Soil Sci. Soc. Am. J.* **2003**, *67*, 606–611.
- (40) Kögel-Knabner, I.; Guggenberger, G.; Kleber, M.; Kandeler, E.; Kalbitz, K.; Scheu, S.; Eusterhues, K.; Leinweber, P. Organo-mineral associations in temperate soils: Integrating biology, mineralogy, and organic matter chemistry. *J. Plant Nutr. Soil Sci.* **2008**, *171*, 61–82.
- (41) Dostal, J.; Breitsprecher, K.; Church, B. N.; Thorkelson, D.; Hamilton, T. S. Eocene melting of Precambrian lithospheric mantle: analcime-bearing volcanic rocks from the Challis–Kamloops belt of south central British Columbia. *J. Volcanol. Geotherm. Res.* **2003**, *126*, 303–326.
- (42) Kiczka, M.; Wiederhold, J. G.; Frommer, J.; Kraemer, S. M.; Bourdon, B.; Kretzschmar, R. Iron isotope fractionation during proton-and ligand-promoted dissolution of primary phyllosilicates. *Geochim. Cosmochim. Acta* **2010**, *74*, 3112–3128.
- (43) Murakami, T.; Utsunomiya, S.; Yokoyama, T.; Kasama, T. Biotite dissolution processes and mechanisms in the laboratory and in

- nature: Early stage weathering environment and vermiculitization. *Am. Mineral.* **2003**, *88*, 377–386.
- (44) Rebertus, R. A.; Weed, S. B.; Buol, S. W. Transformations of biotite to kaolinite during saprolite-soil weathering. *Soil Sci. Soc. Am. J.* **1986**, *50*, 810–819.
- (45) Bortoluzzi, E. C.; Velde, B.; Pernes, M.; Dur, J. C.; Tessier, D. Vermiculite, with hydroxy-aluminium interlayer, and kaolinite formation in a subtropical sandy soil from south Brazil. *Clay Miner.* **2008**, *43*, 185–193.
- (46) Clark, R. B.; Römhild, V.; Marschner, H. Iron uptake and phytosiderophore release by roots of sorghum genotypes. *J. Plant Nutr.* **1988**, *11*, 663–676.
- (47) Andrade, S.; Hypolito, R.; Ulbrich, H. H. G. J.; Silva, M. L. Iron (II) oxide determination in rocks and minerals. *Chem. Geol.* **2002**, *182*, 85–89.
- (48) Dyar, M.; Delaney, J. S.; Sutton, S. R.; Schaefer, M. W. Fe³⁺ distribution in oxidized olivine: A synchrotron micro-XANES study. *Am. Mineral.* **1998**, *83*, 1361–1365.
- (49) Parsons, J. G.; Aldrich, M. V.; Gardea-Torresdey, J. L. Environmental and biological applications of extended X-ray absorption fine structure (EXAFS) and X-ray absorption near edge structure (XANES) spectroscopies. *Appl. Spectrosc. Rev.* **2002**, *37*, 187–222.
- (50) Graham, R. C.; Weed, S.; Bowen, L.; Amarasinghe, D.; Buol, S. Weathering of iron-bearing minerals in soils and saprolite on the North Carolina Blue Ridge Front: II. Clay mineralogy. *Clays Clay Miner.* **1989**, *37*, 29–40.
- (51) Madejová, J.; Komadel, P. Baseline studies of the clay minerals society source clays: infrared methods. *Clays Clay Miner.* **2001**, *49*, 410–432.
- (52) Cocozza, C.; D'oriozio, V.; Miano, T. M.; Shotyk, W. Characterization of solid and aqueous phases of a peat bog profile using molecular fluorescence spectroscopy, ESR and FT-IR, and comparison with physical properties. *Org. Geochem.* **2003**, *34*, 49–60.
- (53) Parker, F. *Applications of Infrared Spectroscopy in Biochemistry, Biology, and Medicine*; Springer Science & Business Media: Berlin, Germany, 2012; pp 21–23.
- (54) Maria, S. F.; Russell, L. M.; Turpin, B. J.; Porcja, R. J. FTIR measurements of functional groups and organic mass in aerosol samples over the Caribbean. *Atmos. Environ.* **2002**, *36*, 5185–5196.
- (55) Gu, B.; Schmitt, J.; Chen, Z.; Liang, L.; McCarthy, J. F. Adsorption and desorption of natural organic matter on iron oxide: mechanisms and models. *Environ. Sci. Technol.* **1994**, *28*, 38–46.
- (56) Carmo, A. M.; Hundal, L. S.; Thompson, M. L. Sorption of hydrophobic organic compounds by soil materials: application of unit equivalent Freundlich coefficients. *Environ. Sci. Technol.* **2000**, *34*, 4363–4369.
- (57) Lv, J.; Zhang, S.; Wang, S.; Luo, L.; Cao, D.; Christie, P. Molecular-scale investigation with ESI-FT-ICR-MS on fractionation of dissolved organic matter induced by adsorption on iron oxyhydroxides. *Environ. Sci. Technol.* **2016**, *50*, 2328–2336.
- (58) Tisdall, J. M.; Oades, J. M. Organic matter and water-stable aggregates in soils. *J. Soil Sci.* **1982**, *33*, 141–163.
- (59) Lehmann, J.; Solomon, D.; Kinyangi, J.; Dathe, L.; Wirick, S.; Jacobsen, C. Spatial complexity of soil organic matter forms at nanometre scales. *Nat. Geosci.* **2008**, *1*, 238–242.
- (60) Michel, F. M.; Ehm, L.; Antao, S. M.; Lee, P. L.; Chupas, P. J.; Liu, G.; Strongin, D. R.; Schoonanen, M. A. A.; Phillips, B. L.; Parise, J. B. The structure of ferrihydrite, a nanocrystalline material. *Science* **2007**, *316*, 1726–1729.
- (61) Tombácz, E.; Libor, Z.; Illés, E.; Majzik, A.; Klumpp, E. The role of reactive surface sites and complexation by humic acids in the interaction of clay mineral and iron oxide particles. *Org. Geochem.* **2004**, *35*, 257–267.
- (62) Vogelmann, E. S.; Reichert, J. M.; Prevedello, J.; Awe, G. O.; Mataix-Solera, J. Can occurrence of soil hydrophobicity promote the increase of aggregates stability? *Catena* **2013**, *110*, 24–31.
- (63) Baker, L. L.; Nickerson, R. D.; Strawn, D. G. XAFS study of Fe-substituted allophane and imogolite. *Clays Clay Miner.* **2014**, *62*, 20–34.
- (64) Scholtzová, E.; Tunega, D.; Turi Nagy, L. Theoretical study of cation substitution in trioctahedral sheet of phyllosilicates. An effect on inner OH group. *J. Mol. Struct.: THEOCHEM* **2003**, *620*, 1–8.
- (65) Tamura, H.; Tanaka, A.; Mita, K.-y.; Furuichi, R. Surface Hydroxyl Site Densities on Metal Oxides as a Measure for the Ion-Exchange Capacity. *J. Colloid Interface Sci.* **1999**, *209*, 225–231.
- (66) Tombácz, E.; Csanyi, C.; Illés, E. Polydisperse fractal aggregate formation in clay mineral and iron oxide suspensions, pH and ionic strength dependence. *Colloid Polym. Sci.* **2001**, *279*, 484–492.
- (67) Vogler, E. A. Structure and reactivity of water at biomaterial surfaces. *Adv. Colloid Interface Sci.* **1998**, *74*, 69–117.
- (68) Totsche, K. U.; Amelung, W.; Gerzabek, M. H.; Guggenberger, G.; Klumpp, E.; Knief, C.; Lehndorff, E.; Mikutta, R.; Peth, S.; Prechtel, A.; Ray, N.; Kögel-Knabner, I. Microaggregates in soils. *J. Plant Nutr. Soil Sci.* **2018**, *181*, 104–136.
- (69) Zhou, Y.; Zhang, Y.; Li, G.; Wu, Y.; Jiang, T. A further study on adsorption interaction of humic acid on natural magnetite, hematite and quartz in iron ore pelletizing process: Effect of the solution pH value. *Powder Technol.* **2015**, *271*, 155–166.
- (70) Johnston, C. T.; Tombácz, E. Surface chemistry of soil minerals. In *Soil Mineralogy with Environmental Applications*; Dixon, J. B., Schulze, D. G., Eds.; Soil Sci. Soc. Am. Inc., 2002; pp 37–67.
- (71) Stockmann, U.; Adams, M. A.; Crawford, J. W.; Field, D. J.; Henakaarchchi, N.; Jenkins, M.; Minasny, B.; McBratney, A. B.; Courcelles, V. d. R. d.; Singh, K.; Wheeler, I.; Abbott, L.; Angers, D. A.; Baldock, J.; Bird, M.; Brookes, P. C.; Chenu, C.; Jastrow, J. D.; Lal, R.; Lehmann, J.; O'Donnell, A. G.; Parton, W. J.; Whitehead, D.; Zimmermann, M. The knowns, known unknowns and unknowns of sequestration of soil organic carbon. *Agric., Ecosyst. Environ.* **2013**, *164*, 80–99.